A study of transport properties of porous anodic aluminium membranes by dynamic atomic force microscopy

Chu Wu[1,2*], Hannah S. Leese[3], Davide Mattia[3], Raymond R. Dagastine[1,4,5], Derek Y.C. Chan[1,2,6¶] and Rico F. Tabor[1,7#]

[1]Particulate Fluids Processing Centre, University of Melbourne, Parkville 3010 VIC, Australia
[2]Department of Mathematics and Statistics, University of Melbourne Parkville 3010 VIC, Australia
[3]Department of Chemical Engineering, University of Bath, Bath, UK
[4]Department of Chemical and Biomolecular Engineering, University of Melbourne, Parkville 3010, Australia
[5]Melbourne Centre for Nanofabrication, 151 Wellington Road, Clayton 3168, Australia
[6]Faculty of Life and Social Sciences, Swinburne University of Technology, Hawthorn 3122, Australia
[7]Department of Chemistry, Monash University, Clayton 3800, Australia

[*]Contributed equally to this work

[¶]D.Chan@unimelb.edu.au
[#]Rico.Tabor@monash.edu.au

Abstract

Carbon nanotubes (CNTs) have recently garnered considerable attention in the area of water treatment due to their observed and predicted enhanced flow rate. Recent work has also demonstrated that porous anodic alumina membranes (PAAMs) which consist of an alumina membrane with hydrophilic nanochannels passing through them can also experience similar enhanced flow and may be an alternative to CNTs. However not a lot of research has focused on PAAMs and a greater understanding of PAAMs is needed if they are to have industrial applications. For this study, we performed a series of experiments using the atomic force microscope (AFM) to probe the hydrodynamic properties on PAAMs with varying pore diameters. These PAAMs can be further categorised as being either 'closed' or 'open' where the back of the PAAMs can be either blocked or unblocked with the latter case allowing fluid to pass through and whilst the former prevents this. The experimental results were compared with a theoretical model that incorporates hydrodynamic forces with possible slip effects, Derjaguin-Landau-Verwey-Overbeek (DLVO) forces and cantilever drag effects. The model was able to accurately describe the 'closed' pore membrane after introducing a slip length whilst also demonstrating that the difference between 'closed' and 'open' pore PAAMs are negligible. Thus we present a simple yet effective model that not only describes the hydrodynamic characteristics of PAAMs but for membranes in general.

1. Introduction

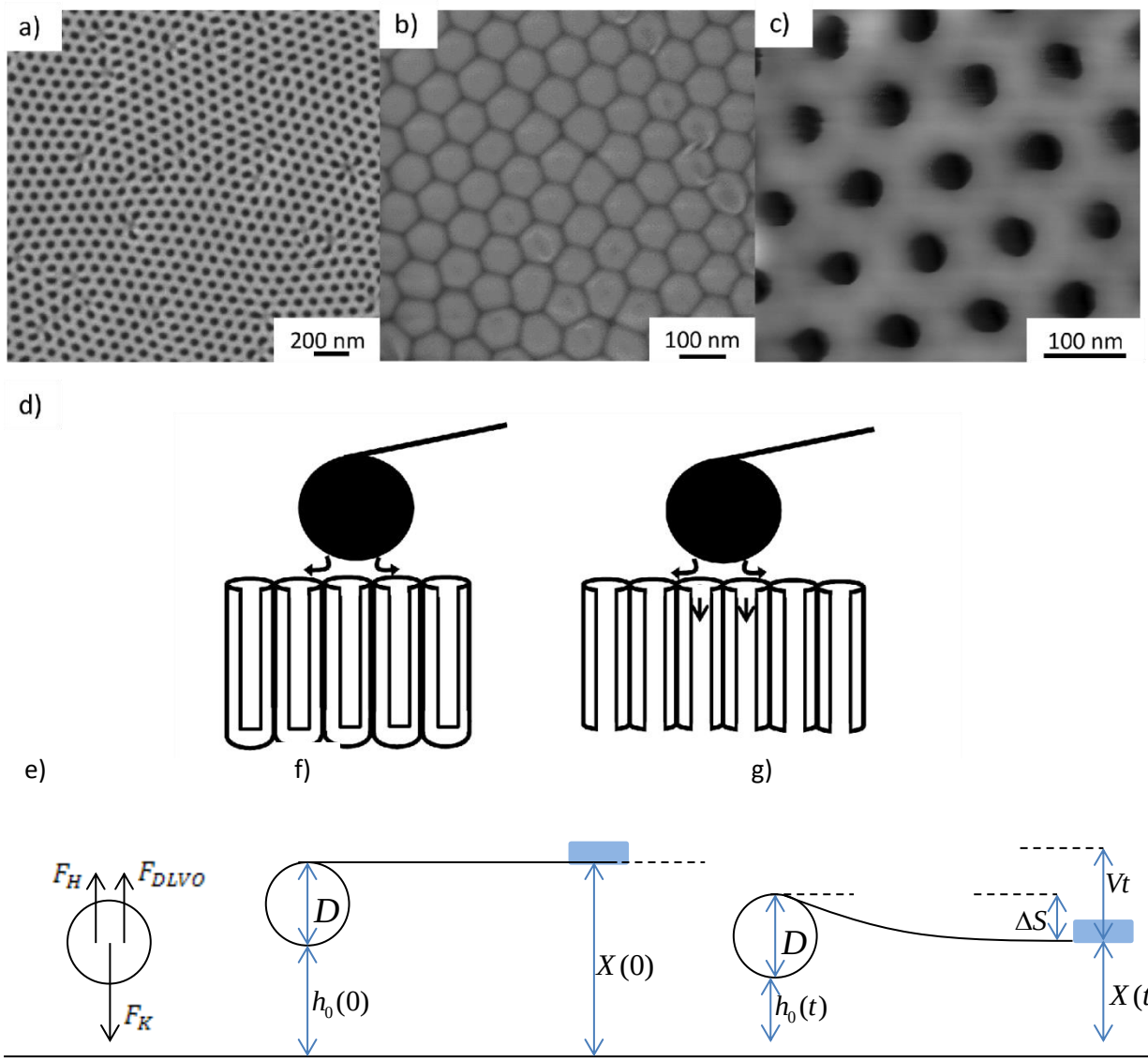

Figure 1 (a-c) FESEM of a porous anodic alumina membrane (PAAMs) at 40V where a) is the top surface that the silica particle was driven into for both the 'closed' and 'open' pore cases, b) is the barrier oxide layer which caps the channels in 'closed' pore samples and c) is a tapping mode AFM image post barrier oxide layer dissolution to give the 'open' pore case. d) is schematic of a cross section of the 'closed' (left image) and 'open' (right image) pore systems. e) is a free body diagram of the forces acting on the particle. f) and g) are diagrams of the atomic force microscope (AFM) with silica particle pushed against the PAAMs with e) being the initial starting position of the system, and f) when the particle is being pushed against the surface which has caused the cantilever to deflect by ΔS.

Over the past few years, research into carbon nanotubes (CNTs) has garnered considerable with the majority of this focus on their potential applications in science and engineering due to their remarkable physical properties. Their incredible strength is of interest to materials and mechanical engineering,[1] whereas their extremely high electrical conductivity is significant to electrical engineering disciplines.[2,3] Recent work has also focused on utilising CNTs embedded in membranes

for water treatment because of the low hydrodynamic resistance of such membranes observed in experimental studies and predicted in molecular simulation.[4–12] Recent work[13] has also demonstrated that hydrophilic nanochannels also exhibit low resistance fluid flow and may be an alternative to CNTs for use in water treatment. The experimental and theoretical work presented in this paper aims to describe the flow around and through these hydrophilic nanochannels and the ideas as well as subsequent analysis presented here will be relevant to understanding flow properties of membranes in general.

In this study, porous anodic alumina membranes (PAAMs) were used as the hydrophilic nanochannels. PAAMs have been utilised in many different applications, such as templates for synthesis procedures[14] and as material in fluid flow studies[13]. The PAAMs used in this study were fabricated at different anodization voltages and this served to produce membranes with different pore diameters as shown in Figure 1(a-c). At the same time these membranes can be characterised as being either 'closed' or 'open' as illustrated in Figure 1d. The left hand image is the 'closed' case with the back of the PAAMs blocked, whilst the image on the right is an example of the 'open' case where the back in now unblocked and thus can allow fluid to pass through.

The present experimental study uses the atomic force microscope (AFM) with a colloid probe to quantify fluid behaviour near the PAAMs surface. The probe is made by gluing a colloidal particle to the tip of the cantilever of the AFM to provide a large surface area to interact with the membrane. This approach is known to be very useful tool for investigating flow on the nanoscale through measuring the hydrodynamic forces.[15] Colloid probes can be driven towards membrane surfaces at varying speeds to measure hydrodynamic interactions. This paper will present experimental results and theoretical analysis on several PAAMs with different pore diameters. Force measurements were conducted on 'closed' and 'open' membranes to determine the potential effects of fluid drainage through membrane pores.

The theoretical model developed as part of this study incorporated van der Waal (vdW) and electrical double-layer (EDL) interactions considered in the Derjaguin-Landau-Verwey-Overbeek (DLVO) theory of colloidal forces.[16] The hydrodynamic interactions between the colloid probe and the membrane is also included as well as the cantilever drag effect that may be important at high AFM drive velocities. The presence of the pores on the membrane surface for the 'open' PAAMs leads to the possibility of flow passing through the membrane and is also incorporated into the modelling.

The presence of nanochannels in the PAAMs means that the membrane surface is not smooth but rather is covered with pores (Figure 1a). As the nanochannels are hydrophilic, these pores will be filled when immersed in water and thus the membrane surface is a solid with varying fraction of liquid regions. Thus, fluid flowing across the surface will encounter a mixture of solid and liquid interfaces that in turn raises the possibility that the no-slip boundary condition which is typically applied on uniformly solid surfaces is no longer applicable on the membrane. Furthermore, for the 'open' membranes the Stokes-Reynolds equation that can be used to derive the hydrodynamic forces for thin films[17] must be modified to account for flow through the membrane and thus a new treatment of the hydrodynamic interaction is required.

The no-slip boundary condition, which assumes that the fluid velocity at the surface is equal to the surface velocity and has been used successfully model Couette and Hagen-Poiseuille flow as well as many other hydrodynamic and engineering systems on the macroscopic scale. It has also been used to successfully describe thin film drainage behaviour at the nano-scale for deformable surfaces.[18] On the other hand the slip condition assumes that fluid velocity at the surface is different from the surface itself and it has been argued that slip does occur for Newtonian fluids at the micro and nano scale.[15]

The idea of a hydrodynamic slip boundary condition in which the tangential velocity of the fluid at an interface is proportional to the tangential stress was first proposed by Navier in 1823.[19,20] This idea has been revived as a convenient model to subsume complex flow conditions at surfaces that arise from surface structures or fluid granularity. For example, Bonaccurso *et al.* examined the hydrodynamic slips using the AFM between a colloidal probe and surfaces with systematically increasing surface roughness.[21] The idea of hydrodynamic slip was proposed as a convenient way to capture this deviation between experimental and the simple model of a smooth, solid no-slip surface. Zhu *et al.* used the AFM to study the hydrodynamic interactions between an OTS-coated silicon wafer and a borosilicate particle in di-n-octylphthalate fluid.[15] Deviations from the no-slip model in this unusual fluid/solid system were attributed to a slip length in the range of 24-31 nm at approach velocities of 10-80 μm/s.[15] More recent work by, Gupta *et al.* made direct force measurements between surfaces with structured cylindrical posts in hexagonal array usinga surface force apparatus (SFA)[22] where they modelled the hydrodynamic drainage behaviour in terms of a deviation function from the no0slip case and employed a scaling analysis to describe the separation at the onset of the deviation.

However it is clear that unless considerable effort is expended to accurately model the details of surface structures or fluid at interfaces (a task that may involve invoking a number of unknown parameters), the idea of slip can be useful to parameterise this complex behaviour if it can help predict the performance of industrial and technological processes, like flow through porous media, particle lubrication, electroosmotic flow as well as better utilisation of micro and nanofluidic devices.[21]

2. Experimental

2.1 Fabrication of Porous Anodic Alumina Membranes (PAAMs)

2.1.1 Closed Pores

A well-established two-step anodization process was carried out for the production of porous anodic alumina membranes (PAAMs).[13,23] High purity (99.99%, 10 mm diameter) aluminium disks (Alfa Aesar) were first annealed in air at 500°C for 60 minutes, degreased in acetone and subsequently electropolished (1:4 v/v $HClO_4$/EtOH) prior to the first step of anodization. The pristine substrates were then anodized at 10-25 V and 30-80 V in 0.5 M sulphuric acid and 0.3 M oxalic acid electrolytes respectively for 30 minutes (see Table 1 for anodization conditions). The alumina formed from the first step was then removed by wet chemical etching using a 1:1 mixture of 6 wt% H_3PO_4 and 1.8 wt% H_2CrO_4 at 60°C for 20 minutes. Immediately after the oxide removal the substrate was anodized again (with the same conditions as its first step) for 5-6 hours for sulphuric and 10-12 hours for the oxalic electrolyte respectively.

2.1.2 Open Pores

To produce the 'open' pore membranes, two additional steps are added to the 'closed' pore procedure outlined above.[13] After obtaining a 'closed' pore sample, the remaining aluminium layer after anodization was removed with a 0.2 M $CuCl_2$/20% HCl mixture to expose the back layer of the alumina which is known as the barrier oxide layer. To achieve the PAAMs with open pores, the barrier oxide layer must be removed and the pores opened. Therefore the PAAMs were exposed to hot (55°C) H_3PO_4 for a period of 5-30 minutes (dependent on pore diameter). A Carl Zeiss XB1540 Gemini® Field Emission Scanning Electron Microscope was used to obtain images shown in Figure 1a) and b), which shows the top surface and the 'closed ' membrane structure. An AFM Veeco Multimode with Nanoscope III controller was used to obtain Figure 1c) which presents the images of 'open' membrane structure post-pore opening.

Anodization Voltage (V)	Electrolyte	Pore Diameter, D_P (nm)	Interpore Distance, D_C (nm)	Porosity K
10	0.5 M H_2SO_4, 0°C	14±2	33±3	0.11
20		25±4	54±4	0.11
25		30±4	64±5	0.15
30		32±3	94±3	0.23
40	0.3 M $C_2H_2O_4$, 14°C	44±2	113±2	0.18
50		52±5	140±3	0.17
60		59±3	163±6	0.11
70		99±6	219±7	0.32

Table 1 The relationship between the anodization voltage, electrolyte composition, temperature and the geometric characteristics of porous anodic alumina membranes (PAAMs)

2.2 Force Measurements

In order to conduct dynamic force measurements on porous anodic alumina membranes (PAAMs), silicon nitride tipless cantilevers were used in the atomic force microscope (AFM). The cantilever spring constants were determined by the method of Hutter and Bechhoefer[24] and were in the range of 0.10-0.15 Nm^{-1}. The AFM measurements were performed on an Asylum MFP-3D AFM driven by an ARC1 controller. The AFM is also equipped with a linear variable differential transformer (LVDT) sensor in the Z-movement direction to allow direct detection of cantilever Z-position during force measurements. This has been shown to be vital for accurate force-displacement measurements because the AFM piezo drive does not always vary linearly with the input voltage to within the required tolerance.[25]

The tipless cantilevers were loaded with approximately 20 µm diameter silica particles. To do this, V-shaped cantilevers were mounted onto the cantilever holder with the aid of a high-magnification optical microscope (Nikon TE2000). The silica particles were distributed onto a glass slide alongside two-part glue (Arladite (F) "30 minute"). The tipless probe ends were dipped into the glue and then moved and lowered to pick up a silica particle. It was important to ensure that only one particle was attached to the probe (smaller particles could become attached onto the end or the side of the cantilever for instance) so that accurate force measurements could be taken. Once the particle-probes had been left to dry, their structure as confirmed by observing the cantilever holder. The cantilever holder had a skirt of Viton® to protect the piezo and electronics from the fluids in the cell.

A range of PAAMs with different pore diameters (as described in Table 1) were used for the dynamic force measurements. Comparisons of the force curves between the closed and open pores were made. To ensure there was no blocking of flow through the pores in the case of open PAAMs, the membranes were suspended across two glass cover slips and placed onto a glass petri dish. To guarantee there was no movement of the membrane when the measurements were taking place as the probe was riven in to the surface, the coverslips were adhered to the bottom of the petri dish with nail varnish. The membranes were also secured to the coverslips using this method. The measurements were performed in a 1 mM NaOH, pH 10 solution and several areas of each membrane were tested at different velocities (from 20-100 µm s^{-1}).

3. Theory

3.1 Particle Force Balance

The theoretical model can be obtained by considering the force balance on the cantilever particle. In the free body diagram shown in Figure 1e), the three primary forces acting on the particle are the hydrodynamic force (F_H), the Derjaguin-Landau-Verwey-Overbeek force (F_{DLVO}) and cantilever spring force (F_K). Since the Reynolds number of this system is very small, inertial forces can be neglected and summing the forces in Figure 1e) gives Equation (1):

$$F_K = F_H + F_{DLVO} \quad (1)$$

3.2 Spring Force and Cantilever Drag

Figure 1f) and g) shows a schematic diagram of the atomic force microscope (AFM). Here $h_0(t)$ is the separation between the particle and the substrate and $h_0(0)$ is the initial separation. D is the particle diameter, ΔS is the cantilever deflection, $X(t)$ is the cantilever at time t and V is the recorded linear variable differential transformer (LVDT) velocity. The AFM experiments were conducted at velocities of around 10-20 μm s^{-1} and as a result the cantilever may be subjected to hydrodynamic drag. Thus the apparent force measured by the AFM (F_{app}) will be a combination of the force on the particle and the cantilever drag. For this model, it is assumed that drag is directly proportional to the product of the cantilever velocity, fluid viscosity and some drag constant term.[26]

$$F_{app} = F_K + F_{drag} = F_K + C\mu\frac{dX}{dt} \quad (2)$$

The C term is the aforementioned drag constant and μ is the fluid viscosity. The apparent force can be linked to the cantilever deflection, ΔS through Hooke's Law with K being the spring constant. Through Figure 1f) and g), it is possible to relate $h_0(t)$ to the known parameters of V and t recorded from the AFM and then merge them with the result in Equation (2) to form Equation (3) below:

$$F_K = K(h_0(t) - h_0(0) - Vt) - C\mu\frac{dX}{dt} \quad (3)$$

3.3 Derjaguin-Landau-Verwey-Overbeek (DLVO) Forces

The Derjaguin-Landau-Verwey-Overbeek (DLVO) component consists of both the electric double layer (EDL) and van der Waal (vdW) forces. Both components are modelled through Derjaguin's approximation that states the force between a spherical colloidal particle (radius R) and a flat plate is $2\pi R$ multiplied by the interaction energy per unit area between two semi-infinite surfaces.[16]

$$F_{DLVO} = 2\pi R W_{EDL} + 2\pi R W_{vdW} \quad (4)$$

The van der Waals interaction energy per unite area (W_{vdW}) is given by

$$W_{vdW} = -\frac{A}{12\pi h^2} \quad (5)$$

Here A is the Hamaker Constant for a silica-water-alumina system which was approximated to be 1.4×10^{-20} J using the approximation of the non0retarding Hamaker Constant as outlined in Israelachvili.[16] The interaction energy for the EDL (W_{EDL}) is found by first implicitly solving the Poisson Boltzmann equation to determine the EDL disjoining pressure using a method described by Chan *et al*[27]. The resulting disjoining pressure had to be integrated numerically as this solution was not in closed form and this will result in W_{EDL}. Substituting this result along with Equation (5) into Equation (4) will yield the following:

$$F_{DLVO} = 2\pi R W_{EDL} - \frac{RA}{6h^2} \quad (6)$$

3.4 Hydrodynamic Forces -Closed Pores

For our system, the hydrodynamic force for a Newtonian fluid with dynamic viscosity of μ can be found through solving the Stokes-Reynolds equation as expressed in Equation (7):

$$\frac{dh}{dt} = \frac{1}{12\mu r}\frac{\partial}{\partial r}\left(rH\frac{\partial P}{\partial r}\right) \quad (7)$$

$$H = \begin{cases} h^3 & \text{No-slip} \\ h^3\left(\frac{h+4b_0}{h+b_0}\right) & \text{Finite-slip} \\ 4h^3 & \text{Infinite-slip} \end{cases} \quad (8)$$

Where b_0 is the slip length and analytical solutions to Equation (7) are given in Equation (9).[28] This equation is essentially Stokes flow with a correction term λ that takes into account the presence of the wall. The correction term is dependent on whether the system is no-slip ($b_0 = 0$), finite-slip (where b_0 equal some finite number) or infinite slip ($b_0 \to \infty$). The solution to all these cases is shown in Equation (9):

$$F_H = 6\pi\mu R^2 \frac{dh}{dt}\lambda \quad (9)$$

$$\lambda = \begin{cases} \frac{1}{h} & \text{No-slip} \\ \frac{1}{4h} + \frac{3}{32b_0^2}\left[(h+4b_0)\log\left(\frac{h+4b_0}{h}\right) - 4b_0\right] & \text{Finite-slip} \\ \frac{1}{4h} & \text{Infinite-slip} \end{cases} \quad (9)$$

3.5 Hydrodynamic Forces-Open Pores

In the open pore PAAMs case, the Stokes-Reynolds equation (see Equation (7)) must be modified to accommodate the possibility of fluid passing through the membrane. The derivation for this is outlined in the Supplementary Information but the modified Stokes Reynolds equation is presented below:

$$\frac{dh}{dt} = \frac{1}{12\mu r}\frac{\partial}{\partial r}\left(rH\frac{\partial P}{\partial r}\right) - \frac{KP}{L} \qquad (10)$$

In Equation (10) the K and L are the porosity and thickness of the PAAMs respectively. Unlike the closed pore PAAMs, there is no closed form analytical solution to Equation (10) so a perturbation solution of the first order was sought. The perturbation solutions for the no-slip and infinite-slip cases are presented in Equation (11) with their derivation found in the Supplementary Information:

$$F_H = 6\pi\mu R^2\frac{dh}{dt}\lambda \qquad (11)$$

$$\lambda = \begin{cases} \frac{1}{h} - \frac{\mu R\alpha}{h^2} & \text{No-slip} \\ \frac{1}{4h} - \frac{\mu R\alpha}{16h^2} & \text{Infinite-slip} \end{cases} \qquad (11)$$

where $\alpha = \frac{K}{L}$ is the ratio of the PAAMs porosity divided by its thickness. If α is equal to zero (that is a membrane with no pores) then the no-slip and infinite-slip solutions in Equation (11) becomes equivalent to the corresponding no-slip and infinite-slip solutions in Equation (9). The α term is typically of the order of 10^{-10} $m^3N^{-1}s^{-1}$ so the right hand perturbation term in Equation (11) is very small. Thus the difference between Equations (11) and (9) for the no-slip and infinite-slip cases is insignificant with the perturbations only becoming important at very small separations. No perturbation solution to the finite-slip case for Equation (10) was found but it will lie somewhere between the no-slip and infinite-slip solutions expressed in Equation (11) and can be approximated by the finite-slip solution in Equation (9) as the difference between the 'open' and 'closed' cases are expected to be negligible.

3.6 Combining the Equations

The equation of motion describing the particle-membrane separation $h_0(t)$ at the centre of the particle is found by combining Equations (1), (3), (6), (9) and (11) to give Equation (12):

$$K(h_0(t) - h_0(0) - Vt) - C\mu V = -6\pi R^2\frac{dh}{dt}\lambda + 2\pi RW_{EDL} - \frac{RA}{6h^2} \qquad (12)$$

Once the experimental LVDT velocity $V(t)$ is given, Equation (12) can be solved numerically.

4. Results and Discussion

4.1 Flat alumina surface

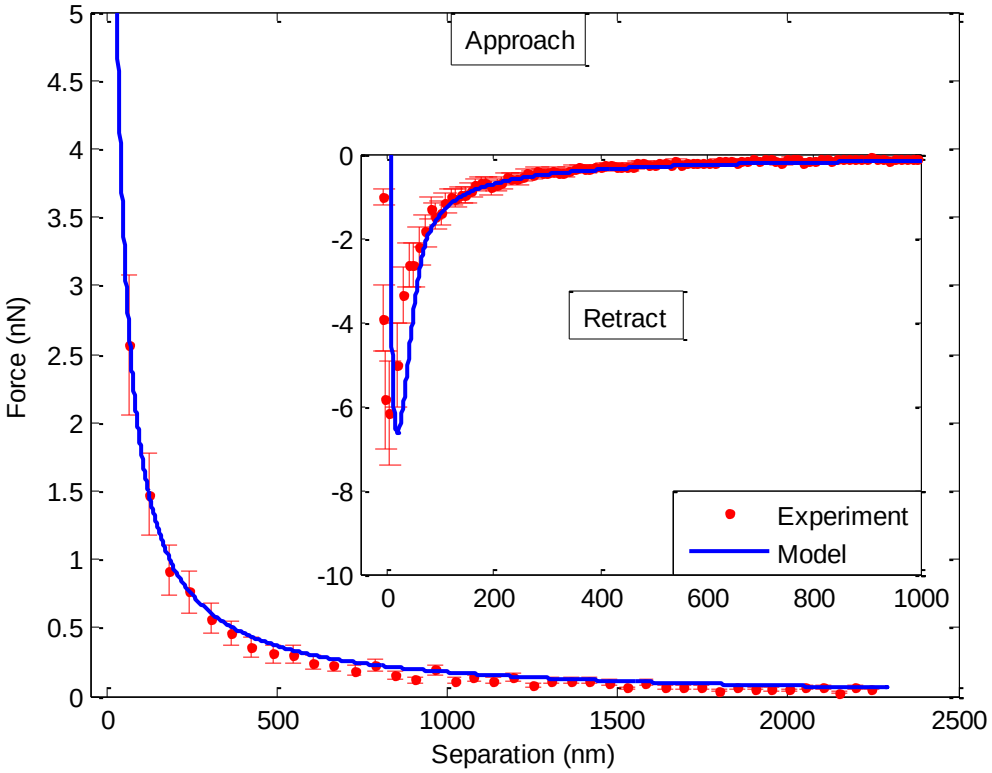

Figure 2 Force against separation ($h_0(t)$) for flat alumina disc driven at nominal speed of 20 µm s^{-1} with a drag constant of 4×10^{-3} m and particle radius of 20 µm. The experiment was conducted in a 0.1 M NaOH solution and modelled using surface potential of -100 mV and viscosity of 0.001 Pa.s. The dots with error bars are the experimental result and the solid curve is the no-slip model solution.

Control experiments were conducted initially on a flat alumina disc. The no-slip boundary condition Was used in the modelling and is presented as the solid curve in Figure 2, where the atomic force microscope (AFM) cantilever was driven at a nominal speed of 20 µm/s. The main plot shows the repulsive fore against separation ($h_0(t)$) during the approach stage and the attractive hydrodynamic force during retraction is shown in the inset. The no-slip model fits the experimental results (dots with error bars) accurately though there is slight deviation at the force minimum on retraction. This may be caused by unknown surface features such as localised surface roughness that interfered with the probe particle at close separations.

4.2 Closed Pores

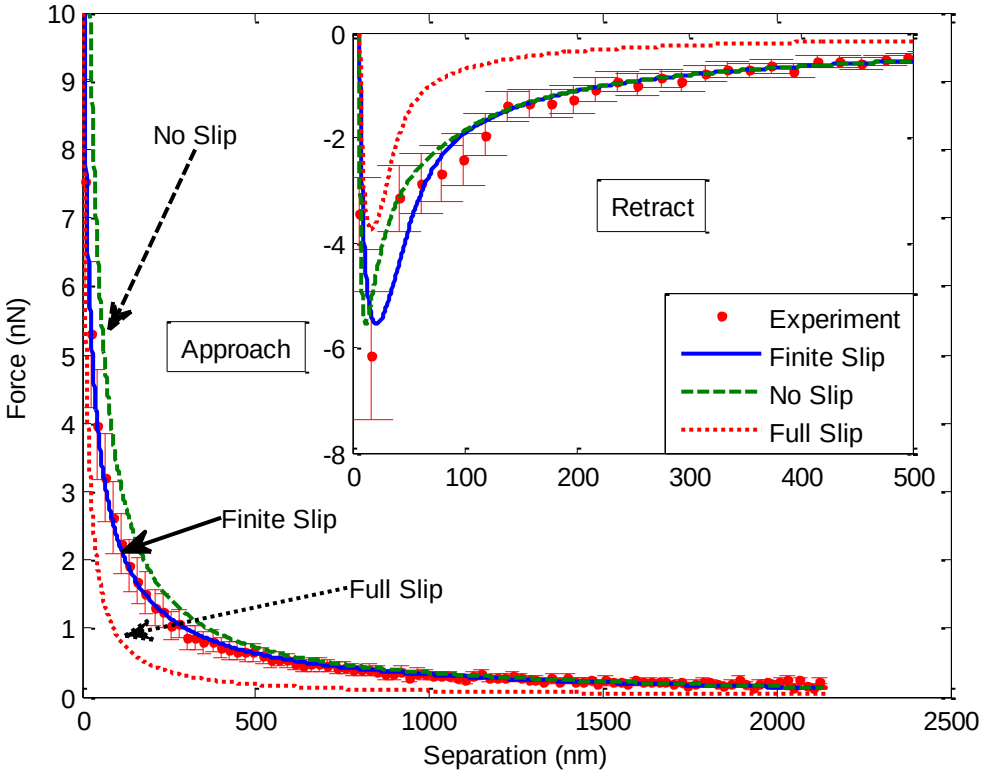

Figure 3 Force against separation curves for porous anodic alumina membrane (PAAMs) with 'closed' pores produced at anodization voltage of 40 V and with pore diameter of 44 ± 2 nm driven at nominal speed of 20 µm s^{-1} with a drag constant of 4×10^{-3} m and particle radius of 20 µm. The experiment was conducted in a 0.1 M NaOH solution and modelled using surface potential of -100 mV and viscosity of 0.001 Pa.s. The dots with error bars are the experimental results and the solid, dashed and dotted curves are the finite-slip, no-slip and full-slip model solutions respectively.

A comparison of the no-slip, full-slip and finite-slip model against the experimental closed pore PAAMs anodised at 40 V (average pore diameter of 44 ± 2 nm_ is shown in Figure 3 at a nominal speed of 40 µm s^{-1}. For these systems the pores are closed off at the back so water can fill the pores but cannot pass through (Figure 1d). The no-slip (dashed) and full-slip (dotted) force curves lie above and below the experimental results respectively. This suggests that a slip model is needed and this is indicated by the solid curve in Figure 3 where a slip length (b_0) of 80 nm was used.

The incorporation of slip length into our model provides a simplistic but convenient way to summarise the variations of the measured hydrodynamic force for membranes with different surface structures. Clearly an *ab inito* prediction of hydrodynamic flow conditions under the differing surface morphologies of the membranes used is a challenging task. Our goal is to seek simple relationships between membrane morphology and flow conditions.

This relationship is highlighted in Figure 4 where large pore diameters have corresponding larger slip lengths. However there is some variability in the model slip length and the range of acceptable

lengths used in the model to approximate the different PAAMs (Figure 4). In part this is due to uncertainties in the pore diameter and the rectangles in Figure 4 shows the diameter and slip length values that lie within the acceptable error tolerances. There appears to be an acceptable linear correlation between the slip length and the pore diameter, with the line passing through the origin that corresponds to the no-slip boundary condition and is expected to hold for PAAMs without pores (Figure 2). However the pore diameter is considerably smaller than the slip lengths used in the modelling and this disparity in length scales suggests that there may be some unknown factors contributing to the slip like behaviour. Nonetheless an *ab initio* derivation of this system will be extremely difficult and using the slip model provides a simple yet reasonably accurate description of the system.

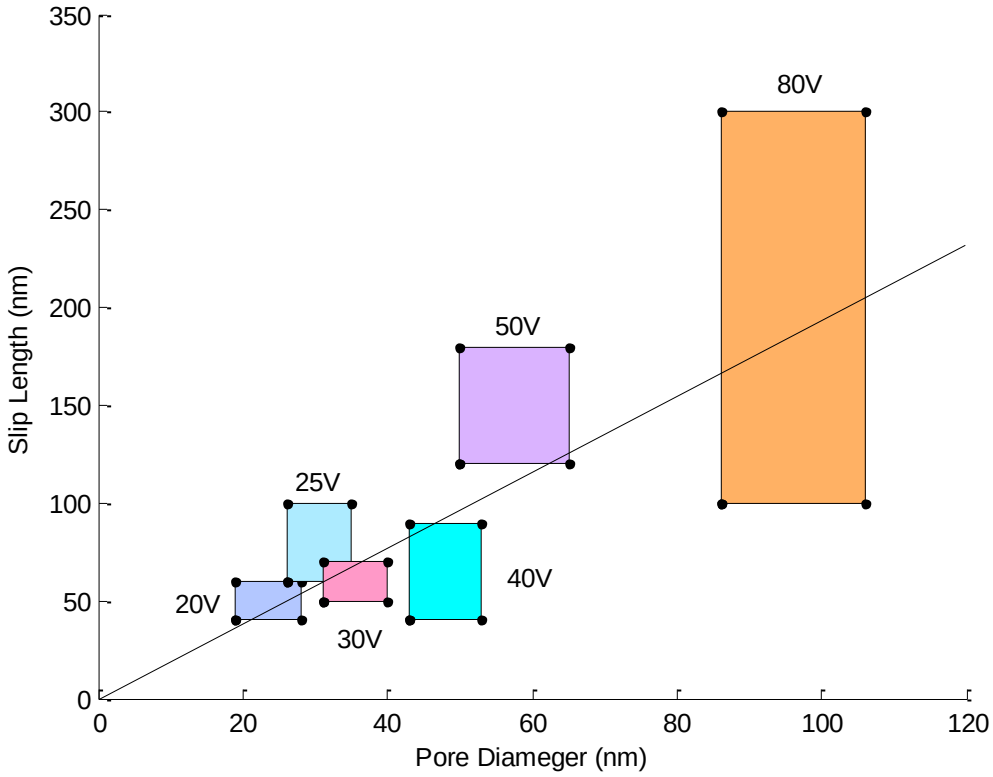

Figure 4 Measured pore diameter with the corresponding model slip lengths for different porous anodic alumina membranes (PAAMs) with closed pores produced at differing anodization voltages.

4.3 Open Pores

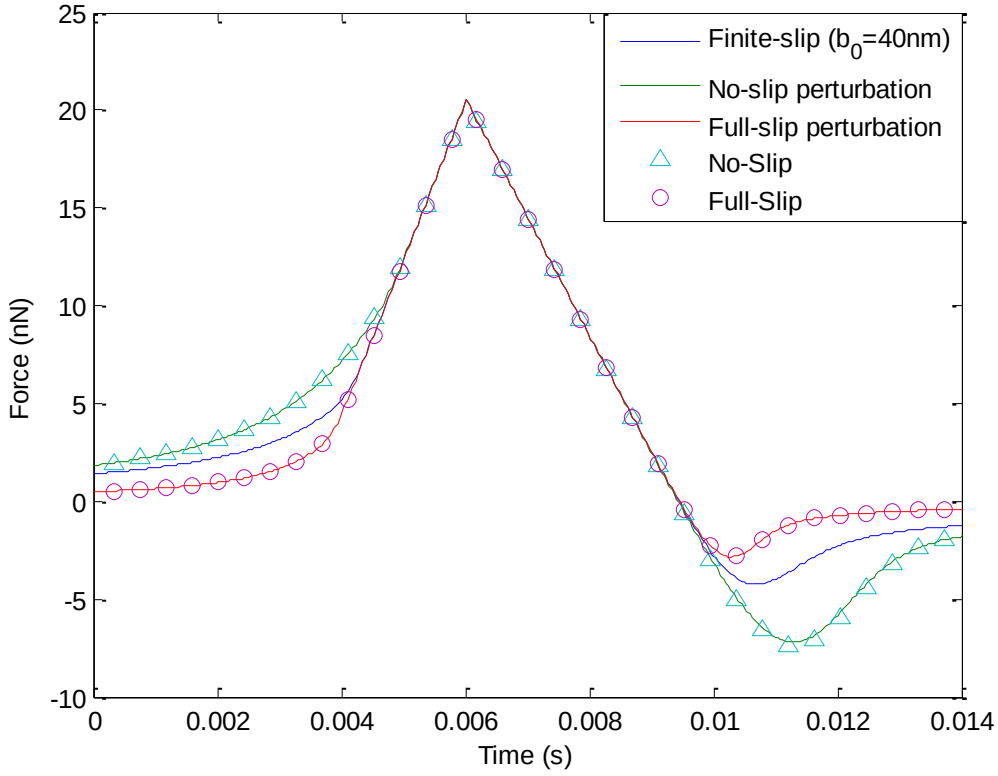

Figure 5 Comparison of perturbation and non-perturbation analytical solutions for open porous anodic alumina membranes (PAAMs) at 40 V with pore diameter of 44 ± 2 nm at nominal speed of 20 µm s^{-1} with a drag constant of 4×10^{-3} m and particle radius of 20 µm. The dashed and dotted lines are the no-slip and full-slip perturbation solutions respectively. The triangle and circles are the no-slip and full-slip non-perturbation solutions respectively. The triangle and circles are the no-slip and full-slip non-perturbation solutions respectively. The solid curve is the finite-slip non-perturbation solution with slip length (b_0) of 40 nm.

A comparison of the non-perturbation solution in Equation (9) and the perturbation solution in Equation (11) reveals that the two equations for the no-slip and full-slip cases differ by the term on the right side of (11) that contains the variable α. This α term is defined as the ratio of the porous anodic alumina membrane (PAAMs) porosity (K) to its thickness (L) and the ratio $\frac{\mu R \alpha}{h}$ is considerably smaller than 1 for most values of separation (h). Thus the difference between Equation (9) and Equation (11) for the no-slip and full-slip cases is negligible.

This is illustrated in Figure 5 where comparisons of the perturbation and non-perturbation solutions for the no-slip and full-slip cases are shown. The non-perturbation solution (triangles and circles for the no-slip and full-slip respectively) lie directly on their corresponding perturbation solutions (dashed and dotted lines for no-slip and full-slip respectively). No perturbation solution for the finite-slip case was found. However it is expected to lie somewhere between the no-slip and full-slip perturbation solutions which are known. Furthermore, since the deviations between the non-

perturbation and perturbation solutions are negligible, it is possible to use the former as an approximation for the latter for finite slip lengths.

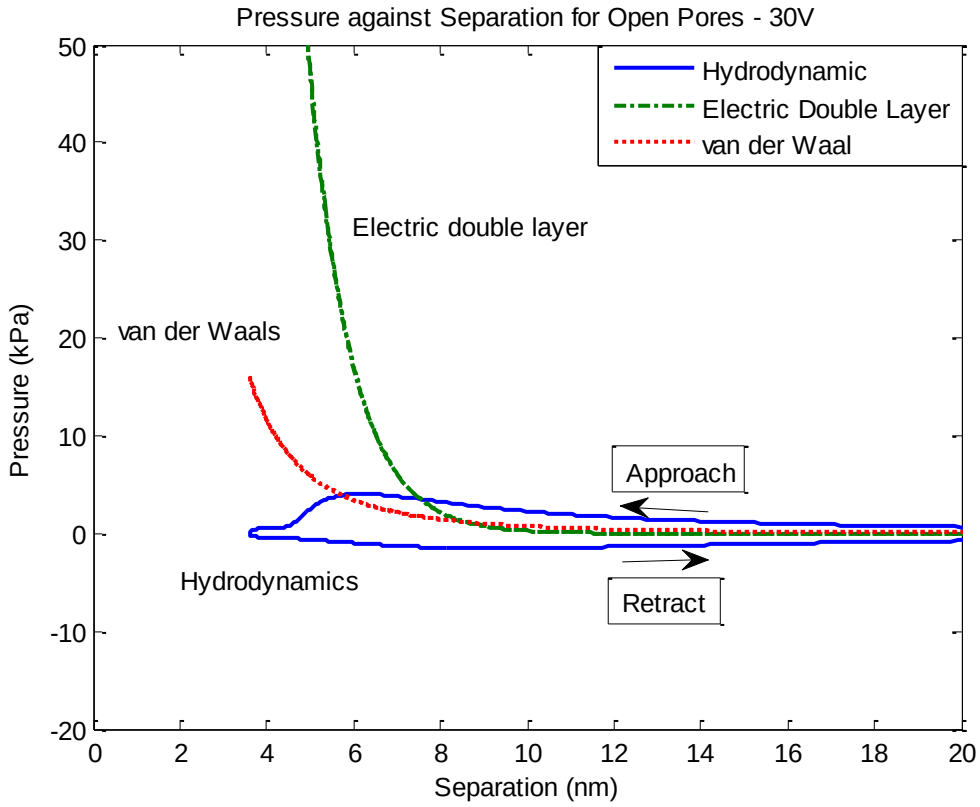

Figure 6 Breakdown of the pressure at the centre of the silica colloid particle calculated from the theoretical model at a nominal speed of 20 µm s^{-1} with a particle size of 20 µm. The modelling was conducted with 0.1 M salt concentration and with both particle and membrane held at a surface potential of -100 mV. The Hamaker constant for the silica-water-alumina system was approximated to be 1.4×10^{-20} J.

To further highlight this, Figure 6 shows the breakdown of the different pressure acting at the centre of the atomic force microscope (AFM) silica particle probe which was calculated using the model. The maximum total pressure is approximately 170 kPa that is outside the vertical scale of Figure 6 and by far the largest contribution is from the electric double layer (EDL) repulsion. As the particle approaches the surface, the separation decreases but at the same time the velocity also falls due to the increasing repulsion caused by the DLVO forces. According to Equations (9) and (11) the hydrodynamic force (and hence hydrodynamic pressure) is inversely proportional to separation but directly proportional to velocity. So as the particle approaches the PAAMs surface, the velocity approaches zero and the hydrodynamic pressure only constitutes a small part of the total pressure with values typically less than 20 kPa. The small hydrodynamic pressure may not be large enough to cause significant flow through the pores. Lee *et al.* found that significant flow through the PAAMs required a hydrodynamic pressure in the order of 100 kPa.[13] So while it is possible there is some flow through the open pores, the very small ydrodynamic pressure suggests it is not the main contributor to the resulting force curves.

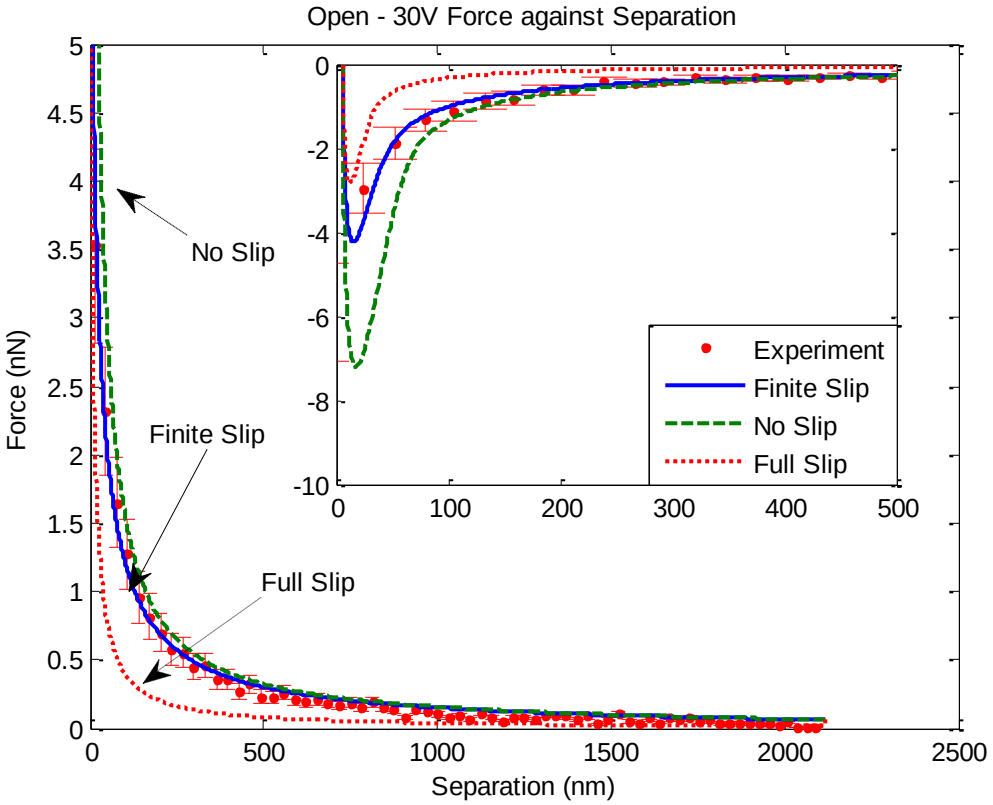

Figure 7 Force against separation curves for porous anodic alumina membranes (PAAMs) with 'open' pores produced at anodization voltage of 30 V and with pore diameter of 32 ± 3 nm at nominal speed of 20 µm s^{-1} with a drag constant of 4×10^{-3} m and particle radius of 20 µm. The experiment was conducted in a 0.1 M NaOH solution and modelled using surface potential of -100 mV and viscosity of 0.001 Pa.s. The dots with error bars are the experimental results and the solid, dashed and dotted curves are the finite-slip, no-slip and full-slip model solutions respectively.

Figure 7 shows the experimental force curves (dots with error bars) for open pore PAAMs anodized at 30 V, which has a relatively small average pore diameter of 32 ± 3 nm. The dashed and dotted lines are the no-slip and full-slip perturbation models respectively and like in Figure 3, these lines bracket the experimental results, thus indicating the need to introduce slip. The finite-slip model (solid curve) is approximated using the closed pore non-perturbation solution and again matches the experiment on approach, though deviates slightly on retract where the experimental minimum is deeper than the model. As in Figure 3, it is believed that localised surface roughness may be the cause for deviation.

In some samples of 'open' pore PAAMs, particularly at large pore sizes, we measure almost no forces until the colloid probe comes into hard contact (constant compliance) with the membrane. We attribute such results to the fact that the final fabrication step in opening the pores (see Section 2.1.2) can result in PAAMs surfaces that are considerably rougher than their 'closed' pore PAAMs counterparts. As a result the colloid probe tends to interact with the tall asperities of the rough membrane surface. This occurs when the result of the membrane is still well separated from the colloid probe with the result that no interaction is detected.

5. Conclusions

Using the atomic force microscope (AFM) to probe the surface of porous anodic alumina membranes (PAAMs) and modelling the experimental results, we were able to gain greater insight into the flow characteristics of these membranes. For 'closed' pore PAAMs, the no-slip boundary condition is no longer applicable as the surface is no longer solid, but rather a mixture of water and alumina. Assuming slip enables the theoretical model to match the experimental results and the slip lengths (b_0) are found to be proportional to PAAMs pore diameter whilst the no-slip boundary condition is expected to hold for a completely flat, featureless surface as they do not have any pores. In the absence of an *ab initio* model to quantify the hydrodynamic complexities of the porous morphology of such a porous membrane, the slip model provides a simple and convenient way to summarise the main hydrodynamic characteristics.

The experimental results for the 'open' pore PAAMs did not differ significantly from the 'closed' pore PAAMs at small pore diameters. However the 'open' nanochannels raise the possibility that fluid can pass through the membrane via the nanochannels and the Stokes-Reynolds equation must be modified to accommodate for this. A perturbation solution for the hydrodynamic pressure was found which suggests that there is little difference between the two cases and also indicates that very little flow is expected to pass through the membrane at these diameters. Thus it is possible to employ the finite-slip boundary condition at these diameters to describe flow parallel to any membrane surface (not just PAAMs) if the pressure perpendicular to the membrane is small. At larger pore sizes, surface roughness effects dominate the force measurement experiments and preclude detailed probing of the hydrodynamic transport through the membrane pores.

Acknowledgements

This work is supported in part by an Australian Research Council Discovery Project Grant. CW is supported by an Australian Postgraduate Award. Infrastructure support provided by the Particulate Fluids Processing Centre is gratefully acknowledged. The authors also acknowledge the UK EPSRC EP/6045798/1 and EP/J015504/1 for funding. Microscopy and Analysis Suite at the University of Bath and NanoAccess in Cardiff, EPSRC [EP/F056745/1].

Bibliography

1. Dalton, A. B. *et al.* Super-tough carbon-nanotube fibres. *Nature* **423**, 703 (2003).

2. Mattia, D., Rossi, M., Ye, H. & Gogotsi, Y. In situ fluid studies in carbon nanotubes with diameters ranging from 1 to 500 nm. *… international conference on fluid …* 294–296 (2007).at <http://www.wseas.us/e-library/conferences/2007athensmech/papers/565-201.pdf>

3. Ebbesen, T. . *et al.* Electrical Conductivity of Individual Carbon Nanotubes.pdf. 54–56 (1996).

4. Supple, S. & Quirke, N. Molecular dynamics of transient oil flows in nanopores I: Imbibition speeds for single wall carbon nanotubes. *The Journal of chemical physics* **121**, 8571–9 (2004).

5. Supple, S. & Quirke, N. Rapid Imbibition of Fluids in Carbon Nanotubes. *Physical Review Letters* **90**, 214501 (2003).

6. Joseph, S. & Aluru, N. R. Why are carbon nanotubes fast transporters of water? *Nano letters* **8**, 452–8 (2008).

7. Thomas, J. & McGaughey, A. Water Flow in Carbon Nanotubes: Transition to Subcontinuum Transport. *Physical Review Letters* **102**, 184502 (2009).

8. Thomas, J. A. & Mcgaughey, A. J. H. Through Carbon Nanotubes. *Nano letters* **8**, 2788–2793 (2008).

9. Whitby, M., Cagnon, L., Thanou, M. & Quirke, N. Enhanced fluid flow through nanoscale carbon pipes. *Nano letters* **8**, 2632–7 (2008).

10. Majumder, M., Chopra, N., Andrews, R. & Hinds, B. J. Enhanced flow in carbon nanotubes. *Nature* **438**, 44 (2005).

11. Corry, B. Water and ion transport through functionalised carbon nanotubes: implications for desalination technology. *Energy & Environmental Science* **4**, 751 (2011).

12. Kannam, S. K., Todd, B. D., Hansen, J. S. & Daivis, P. J. How fast does water flow in carbon nanotubes? *The Journal of Chemical Physics* **138**, 094701 (2013).

13. Lee, K. P., Leese, H. & Mattia, D. Water flow enhancement in hydrophilic nanochannels. *Nanoscale* **4**, 2621–7 (2012).

14. Martin, C. R. Nanomaterials: a membrane-based synthetic approach. *Science (New York, N.Y.)* **266**, 1961–6 (1994).

15. Zhu, L., Attard, P. & Neto, C. Reliable measurements of interfacial slip by colloid probe atomic force microscopy. I. Mathematical modeling. *Langmuir : the ACS journal of surfaces and colloids* **27**, 6701–11 (2011).

16. Israelachvili, J. *Intermolecular and Surface Forces*. 161–164 (1992).

17. Chan, D. Y. C., Klaseboer, E. & Manica, R. Theory of non-equilibrium force measurements involving deformable drops and bubbles. *Advances in colloid and interface science* **165**, 70–90 (2011).

18. Dagastine, R. R. *et al.* Dynamic forces between two deformable oil droplets in water. *Science (New York, N.Y.)* **313**, 210–3 (2006).

19. Navier, C. L. M. H. No Title. *Mem. Acad. Sci. Inst. FR* **6**, 432–436 (1823).

20. Navier, C. L. M. H. No Title. *Mem. Acad. Sci. Inst. FR* **6**, 389–416 (1823).

21. Bonaccurso, E., Butt, H.-J. & Craig, V. S. Surface Roughness and Hydrodynamic Boundary Slip of a Newtonian Fluid in a Completely Wetting System. *Physical Review Letters* **90**, 1–4 (2003).

22. Gupta, R. & Fréchette, J. Measurement and scaling of hydrodynamic interactions in the presence of draining channels. *Langmuir : the ACS journal of surfaces and colloids* **28**, 14703–12 (2012).

23. Masuda, H. & Fukuda, K. Ordered metal nanohole arrays made by a two-step replication of honeycomb structures of anodic alumina. *Science (New York, N.Y.)* **268**, 1466–8 (1995).

24. Hutter, J. L. & Bechhoefer, J. Calibration of atomic-force microscope tips. *Review of Scientific Instruments* **64**, 1868 (1993).

25. Manor, O. *et al.* Dynamic Forces between Bubbles and Surfaces and Hydrodynamic Boundary Conditions. *Langmuir* **110**, 11533–11543 (2008).

26. Dagastine, R. R. *et al.* Viscosity effects on hydrodynamic drainage force measurements involving deformable bodies. *Langmuir : the ACS journal of surfaces and colloids* **26**, 11921–7 (2010).

27. Chan, D. Y. C., Healy, T. W., Supasiti, T. & Usui, S. Electrical double layer interactions between dissimilar oxide surfaces with charge regulation and Stern-Grahame layers. *Journal of colloid and interface science* **296**, 150–8 (2006).

28. Vinogradova, O. I. Drainage of a Thin Liquid Film Confined between Hydrophobic Surfaces. *Langmuir* **11**, 2213–2220 (1995).